A SEARCH FOR FAINT COMPANIONS TO NEARBY STARS USING THE WIDE FIELD PLANETARY CAMERA 2

DANIEL J. SCHROEDER,[1] DAVID A. GOLIMOWSKI,[2] RYAN A. BRUKARDT,[2] CHRISTOPHER J. BURROWS,[3,4] JOHN J. CALDWELL,[5] WILLIAM G. FASTIE,[2] HOLLAND C. FORD,[2] BRIGETTE HESMAN,[5] ILONA KLETSKIN,[5] JOHN E. KRIST,[3] PATRICIA ROYLE,[3] AND RICHARD. A. ZUBROWSKI[2]

ABSTRACT

We have completed a direct-imaging search for faint companions (FCs) to 23 stars within 13 pc of the Sun using the *Hubble Space Telescope* Planetary Camera. The strategy of this search changed considerably from that reported in 1996. To maximize the image contrast between potential FCs and a target star's point-spread function, we adopted the F1042M filter ($\lambda_c \sim 1.02$ μm, $\Delta\lambda \sim 0.04$ μm) as the primary bandpass of our search. Although our sensitivity to FCs varied with the brightness of and separation from our target stars, an ultimate 10 σ detection limit of $m_{1042} \approx 18$ within 17″ of the fainter targets was achieved. As the end of the main sequence occurs at $M_{1042} \approx 12$, this detection limit makes our search for FCs to nearby stars the most sensitive yet published. Despite this great sensitivity, no previously undetected FCs were found. Our survey would have detected all stellar companions within 17″ of our target stars, except for any lowest mass companions lying within 0″.5–1″ of the brightest ($V < 1.5$) targets. Applying recent models of brown dwarf spectra and evolution, we find that our search was sensitive to young (0.5 Gyr), low-mass (less than 10 M_J) brown dwarf companions to the fainter targets within 5 pc. A brown dwarf with mass 40 M_J and age 5 Gyr would have been detected at separations greater than 5″ from Gl 559A (α Centauri A). Our search was not sensitive to 1 Gyr–old brown dwarfs with masses $\lesssim 5$ M_J, nor was it sensitive to 5 Gyr–old brown dwarfs with masses $\lesssim 10$ M_J. On the positive side, we show the first direct image of the triple system GJ 1245ABC in which all three components are well resolved. Multiband photometry of GJ 1245C suggests for that object a spectral type later than M7. The measured positions of GJ 1245AC are discordant with those expected from published photocentric-orbit elements. The observed positions of four other multiple systems (Gl 65AB, Gl 244AB, Gl 280AB, and Gl 866ABC) also differ from those expected from published orbital elements. The discrepancies noted for Gl 280AB are sufficient to resolve the long-standing inconsistency between Procyon's observed luminosity and that derived from the theoretical mass-luminosity relation. F1042M images of the astrometric binary Gl 105A do not reveal the presence of a fourth component, as has been proposed to reconcile the differences between the observed location of the M7 V companion Gl 105C and the predicted separations of the perturbing body from two independent astrometric studies.

Key words: binaries: close — stars: individual (GJ 1245ABC, Gl 105AC, Procyon) — stars: low-mass, brown dwarfs

1. INTRODUCTION

Direct searches for faint, low-mass companions to stars have been undertaken using a variety of observing techniques, e.g., near-infrared imaging (Probst & O'Connell 1982; Jameson, Sherrington, & Giles 1983; Skrutskie, Forrest, & Shure 1989; Zuckerman & Becklin 1992; Simons, Henry, & Kirkpatrick 1996), mid-infrared imaging (van Buren et al. 1998), near-infrared speckle imaging (Henry & McCarthy 1990; Leinert et al. 1997), optical coronagraphy (Nakajima et al. 1994; Oppenheimer 1999),

and direct optical and near-infrared imaging with the *Hubble Space Telescope* (*HST*; Schroeder & Golimowski 1996, hereafter Paper I; Reid & Gizis 1997b; Krist et al. 1998; Lowrance et al. 1999). These techniques have enjoyed limited success, the most notable being the discovery of the cool brown dwarf Gl 229B (Nakajima et al. 1995).

We have completed a direct-imaging search for faint companions (FCs) to 23 stars within 13 pc of the Sun using the Planetary Camera (PC) of the *HST* Wide Field Planetary Camera 2 (WFPC2). A description of this program, including a characterization of the PC's point-spread function (PSF), the development of an algorithm for identifying FCs near the bright target stars, and an initial observing strategy, was reported in Paper I. We now report the changes in the observing strategy made since Paper I and the detection of no new FCs to the stars in our program. We present the first direct images and multiband optical photometry of the very low mass (VLM) object GJ 1245C. We also report the relative positions of several multiple-star systems in our target sample and compare the positions with those expected from recently published orbital ele-

[1] Department of Physics and Astronomy, Beloit College, Beloit, WI 53511.

[2] Department of Physics and Astronomy, Johns Hopkins University, Baltimore, MD 21218.

[3] Space Telescope Science Institute, 3700 San Martin Drive, Baltimore, MD 21218.

[4] Astrophysics Division, Space Science Department, European Space Agency.

[5] Department of Physics and Astronomy, York University, 4700 Keele Street, Toronto M3J 1P3, ON, Canada.

ments. Finally, we discuss the physical interpretation of our detection limits and the implications of our null result for the frequency of FCs in the solar neighborhood.

2. OBSERVATIONS AND IMAGE ANALYSIS

2.1. Revised Bandpasses and Target Stars

The original strategy for our FC search involved recording several PC images of each target star through two broadband filters, typically F555W and F814W (WFPC2 V and I, respectively; Burrows et al. 1995) and at two epochs separated usually by a few weeks (see Paper I for details). By overexposing the target stars to an integrated signal of 10^8–10^9 e^-, the PC images were saturated to the desired inner search radius of $0\rlap{.}''5$–$1''$ from each star. Multiple images (up to 56 for some bright targets) were then summed to improve the signal-to-noise ratio (S/N) and therefore the probability of finding a FC in the wings of the target's PSF. Two visits to each target were required to confirm any candidate FCs by common proper motion.

Using a search algorithm that identified point sources embedded in the target's PSFs, we adopted a detection limit for FCs of 10 σ above the local background anywhere in the field of view (Paper I). We determined from this 10 σ limit that searching for extrasolar Jovian planets with the PC was nearly impossible, but a brown dwarf as faint as $M_I \sim$ 16.7 could be detected as close as $1''$ from Gl 559B (α Centauri A). We based these determinations on the S/N criterion alone; we did not require a minimum contrast between the brightness of a potential FC and the local background. The S/N criterion itself is valid at large distances from the target stars, where the target's PSF varies smoothly and photon noise dominates the fluctuations of the local background. However, the image contrast between a FC and the target's PSF becomes important within a few arcseconds of the targets, where the brightness variations of the PSF are larger than the local 10 σ detection limit. Because of the large variations of the PSF (see Paper I for a thorough analysis), the image contrast should exceed unity to ensure credible detection of FCs within the imaged field.

TABLE 1
TARGETS OF WFPC2 FAINT-COMPANION SEARCH PROGRAM

Target No. (1)	CNS3 Name (2)	Alternate Name (3)	Observing Group (4)	d (pc) (5)	μ (arcsec yr^{-1}) (6)	V (7)	M_V (8)	Spectral Type (9)
1	Gl 551	Proxima Centauri	4	1.295 (1)	3.853 (1)	11.09 (2)	15.53	M5.5 Ve (3)
2	Gl 559A	α Centauri A	3A	1.347 (1)	3.710 (1)	0.01 (4)	4.36	G2 V (4)
3	Gl 559B	α Centauri B	3A	1.347 (1)	3.724 (1)	1.34 (4)	5.69	K0 V (4)
4	Gl 699	Barnard's Star	4	1.833 (5)	10.358 (1)	9.53 (6)	13.21	M4 V (7)
5	Gl 406	Wolf 359	1A	2.386 (5)	4.696 (4)	13.44 (6)	16.55	M6 V (7)
6	Gl 411	Lalande 21185	1B	2.548 (1)	4.802 (1)	7.47 (2)	10.44	M2 V (7)
7	Gl 244A	Sirius	3B	2.637 (1)	1.339 (1)	−1.43 (4)	1.46	A1 V (4)
	Gl 244B	Sirius B	...	2.637 (1)	1.339 (1)	8.44 (4)	11.33	DA2 (4)
8	Gl 65A	L726-8 A	1A	2.676 (5)	3.368 (4)	12.54 (8)	15.40	M5.5 V (7)
	Gl 65B	L726-8 B	...	2.676 (5)	3.368 (4)	12.99 (8)	15.85	M6 V (7)
9	Gl 729	Ross 154	1A	2.972 (1)	0.666 (1)	10.43 (6)	13.06	M3.5 V (7)
10	Gl 905	Ross 248	1A	3.165 (5)	1.617 (4)	12.29 (6)	14.79	M5.5 V (7)
11	Gl 144	ϵ Eridani	2B	3.218 (1)	0.977 (1)	3.73 (4)	6.19	K2 V (4)
12	Gl 447	Ross 128	1A	3.353 (5)	1.361 (1)	11.13 (6)	13.50	M4 V (7)
13	Gl 866AC	L789-6 AC	1A	3.454 (5)	3.254 (4)	12.85 (8)	15.16	M5 V^a (7)
	Gl 866B	L789-6 B	...	3.454 (5)	3.254 (4)	13.27 (8)	15.58	...
14	Gl 820A	61 Cygni A	2A	3.486 (5)	5.281 (1)	5.21 (4)	7.50	K5 V (7)
	Gl 820B	61 Cygni B	...	3.504 (1)	5.172 (1)	6.03 (2)	8.31	K7 V (7)
15	Gl 280A	Procyon	3A	3.497 (1)	1.259 (1)	0.38 (4)	2.66	F5 IV-V (4)
	Gl 280B	Procyon B	...	3.497 (1)	1.259 (1)	10.7 (4)	13.0	DA (4)
16	Gl 725A	HD 173739	1B	3.506 (5)	2.313 (1)	8.90 (6)	11.18	M3 V (7)
	Gl 725B	HD 173740	...	3.506 (5)	2.313 (1)	9.69 (6)	11.97	M3.5 V (7)
17	Gl 15A	HD 1326A	1B	3.568 (1)	2.918 (1)	8.08 (2)	10.32	M1.5 V (7)
	Gl 15B	HD 1326B	...	3.568 (1)	2.918 (1)	11.06 (6)	13.30	M3.5 V (7)
18	Gl 845	ϵ Indi	^{b}	3.626 (1)	4.704 (1)	4.69 (4)	6.89	K5 Ve (4)
19	Gl 71	τ Ceti	2B	3.647 (1)	1.922 (1)	3.49 (4)	5.68	G8 Vp (4)
20	GJ 1245A	G208-44 A	1A	4.541 (5)	0.731 (4)	13.47 (8)	15.18	M5.5 V^c (7)
	GJ 1245B	G208-45	...	4.541 (5)	0.731 (4)	14.01 (6)	15.72	M6 V (7)
	GJ 1245C	G208-44 B	...	4.541 (5)	0.731 (4)	16.76 (8)	18.47	...
21	Gl 440	L145-141	4	4.621 (1)	2.688 (1)	11.50 (4)	13.18	DQ6 (4)
22	Gl 768	Altair	3A	5.143 (1)	0.661 (1)	0.77 (4)	2.21	A7 IV-V (4)
23	Gl 105A	HD 16160	4	7.209 (1)	2.312 (1)	5.82 (4)	6.53	K3 V (4)
	Gl 105C	...	...	7.209 (1)	2.312 (1)	16.9 (9)	17.6	...
24	Gl 395	36 Ursae Majoris A	4	12.85 (1)	0.180 (1)	4.84 (4)	4.30	F8 V (4)

NOTE.—References are indicated in parentheses in cols. (5)–(7) and (9).

^{a} Combined spectral type for components A, B, and C.

^{b} All observations of Gl 845 (ϵ Indi) were lost because of failed guide-star acquisition.

^{c} Combined spectral type for components A and C.

REFERENCES.—(1) ESA 1997; (2) Leggett 1992; (3) Hawley, Gizis, & Reid 1996, 1997; (4) Gliese & Jahreiss 1991, hereafter CNS3; (5) van Altena, Lee, & Hoffleit 1995; (6) Weis 1996; (7) Henry, Kirkpatrick, & Simons 1994; (8) Henry et al. 1999; (9) Golimowski et al. 1995a.

The extreme redness of VLM stars and brown dwarfs at optical wavelengths (Leggett 1992; Golimowski & Schroeder 1998; Leggett, Allard, & Hauschildt 1998) indicates that the largest contrast between the images of potential FCs and a target's PSF is achieved through the reddest WFPC2 filter, F1042M ($\lambda_c \sim 1.02$ μm, $\Delta\lambda \sim 0.04$ μm; Burrows et al. 1995). Moreover, the rapidly rising brightness of Gl 229B through progressively redder WFPC2 filters (Golimowski et al. 1998) shows that WFPC2's sensitivity to cool brown dwarfs through F1042M is not significantly impaired, despite its low efficiency (0.36% peak) in that bandpass. Therefore, in early 1996, we changed the primary filters of our FC search from F555W and F814W to the redder combination of F814W and F1042M.

The balance of *HST* orbits in our program permitted the reexamination of the original 18 targets in our program (see Table 1 of Paper I) plus the observation of six other nearby stars through the revised complement of filters. The complete and final list of target stars is presented in Table 1. The six new targets were selected so that our program would include the 17 star systems nearest the Sun. This plan was short lived, however, as the subsequent release of the *Hipparcos* output catalog significantly altered the order of the nearest stars. Table 1 lists our targets in order of increasing distance from the Sun, as determined from the latest releases of the Yale and *Hipparcos* catalogs of parallaxes (van Altena, Lee, & Hoffleit 1995; ESA 1997).

2.2. Revised Observing Strategy

The change in bandpasses made necessary other changes in our observing strategy so that the target stars would be examined in a consistent manner. The 24 targets were segregated into four groups based on apparent brightness and observing history. The targets thus resided in group 1 ($V > 7.5$), group 2 ($3 < V < 5.2$), group 3 ($V < 1.5$), or group 4 (miscellaneous). The faintest targets (group 1) were imaged through F1042M, F814W, and F675W (WFPC2 *R*) with individual exposure times of 400, 100, and 100 s, respectively. These times defined the deepest exposures for images taken through these filters. The F675W images were recorded for additional color discrimination of FC candidates at a detection limit similar to that of the F814W images ($m \approx 22.5$). For the targets of intermediate brightness (group 2), images were obtained through F1042M and F814W that were saturated within $\sim 0\rlap{.}''5$ and $\sim 1''$ of the stars' positions. For the brightest targets in group 2, the narrowband filter F953N ($\lambda_c \approx 954$ nm, $\Delta\lambda \approx 0.5$ nm; Burrows et al. 1995) was used instead of the broadband F814W to obtain a second set of images saturated within $\sim 0\rlap{.}''5$ of the stars. (F953N and F1042M have the same integrated efficiency with respect to the WFPC2 CCDs.) The brightest targets in our program (group 3) were imaged through F1042M and F953N only, using exposure times that produced saturation within $0\rlap{.}''5-2''$ of the stars' positions. Short exposures of all the target stars were recorded through F1042M so that unsaturated or minimally saturated images of the targets themselves could be obtained for astrometric purposes.

The observing group into which each target was placed is listed in column (4) of Table 1. The sets of exposures for groups 1–3 are outlined in Table 2. Each group has been divided into subgroups A and B according to target brightness so that different exposure sets within each group are clearly noted. The exposure sets were designed to maximize

the sensitivity of the F1042M and F814W images to Gl 229B–like FCs, while keeping the entire set within the length of one *HST* orbit. Because the exposure times per filter and the levels of scattered light from the targets' PSFs vary significantly among these groups, the sensitivity to FCs also varies groupwise. The estimated FC detection limits as a function of distance from the targets within each group are discussed in § 3.1. The exposure sets for the targets in group 4 are described in § 2.3.

The exposure set for each target except Gl 395 was executed once during each of two *HST* visits to the target. These visits were separated by a time interval within which the target moved at least $0\rlap{.}''23$ (5 PC pixels) with respect to the fixed celestial background. This epochal separation was deemed sufficient to allow easy discrimination of distant background sources from FCs having proper motion similar to that of the target. To ease the scheduling of the visits, we dropped a previously imposed constraint of having the same spacecraft roll for each visit (Paper I). Consequently, our targets were no longer guaranteed to be imaged at the same location or orientation on the detector. The visits to Gl 905 and Gl 820AB were separated by 11 and 17 months, respectively, because of *HST* or guide-star acquisition problems. Both visits to Gl 845 were aborted because of guide-star acquisition failures and were never rescheduled.

2.3. Observations of Group 4 Targets

Many of our target stars had been observed extensively using the observing strategy described in Paper I. Some of the exposures from these earlier observations were relevant to the revised observing strategy described above and therefore did not require repeating. Consequently, the exposure sets for five targets do not conform exactly to the observing strategies for groups 1–3. The observations of these five group 4 targets are now discussed individually.

Gl 551 (Proxima Centauri).—Three visits to Gl 551 were performed prior to the adoption of the revised observing strategy. During these visits, sets of eight 40 and 200 s exposures through F814W were recorded, and sets of eight 120 and 600 s exposures through F675W were obtained. These sets of exposures provided deep images of the target field beyond $0\rlap{.}''25$ and $0\rlap{.}''5$ from Gl 551, respectively. During visits 4 and 5, the observing strategy was the same as listed in Table 2 for group 2A, except that the F814W exposures were omitted and the shortest F1042M exposures were each 10 s.

Gl 699 (Barnard's Star).—The observations over five visits to Gl 699 mimicked those described above for Gl 551. Images through F814W were recorded for exposure times of 8, 40, and 200 s, and images through F675W were recorded for exposure times of 23, 120, and 600 s. These exposures resulted in images saturated within $0\rlap{.}''25$, $0\rlap{.}''5$, and $0\rlap{.}''75$ of Gl 699, respectively. The F1042M exposures matched those for group 2A, except that the shortest F1042M exposures were each 1.6 s.

Gl 440 (L145–141).—Four visits to Gl 440 were executed during our program. Sets of three images were recorded through F814W and F675W during each of the first two visits. These exposure times of 300 and 260 s, respectively, produced images saturated within $0\rlap{.}''25$ of the star. The exposure sets for visits 3 and 4 were the same as those for the group 1A targets, except that 40 s exposures were recorded through F814W and F675W.

TABLE 2
EXPOSURE SETS FOR OBSERVING GROUPS 1–3

Observing Group	Target Brightness	No. of Targets	WFPC2 Filter	Exposure Time (s)	No. of Exposures	Gain ($e^- \, DN^{-1}$)	Comments
1A	$V > 10$	7	F1042M	≤ 40	2–3	7 or 14	Unsaturated image
			F1042M	400	2	7	FC search to $m \approx 18$
			F814W	100	3–4	7	FC search to $m \approx 22.5$
			F675W	100	4	7	FC search to $m \approx 22.5$
1B	$7.5 < V < 10$	3	F1042M	<1	2	7 or 14	Unsaturated image
			F1042M	400	2	7	Saturated to $\sim 0\rlap{.}''5$
			F814W	14–16	3	7	Saturated to $\sim 0\rlap{.}''5$
			F814W	100	3–4	7	Saturated to $\sim 1''$
			F675W	14–16	3	7	Saturated to $\sim 0\rlap{.}''5$
			F675W	100	2–3	7	Saturated to $\sim 1''$
2A	$4.7 < V < 5.2$	2	F1042M	0.2	1	14	Minimally saturated
			F1042M	40	3	14	Saturated to $\sim 0\rlap{.}''35$
			F1042M	400	3	14	Saturated to $\sim 0\rlap{.}''7$
			F953N	40	3	14	Saturated to $\sim 0\rlap{.}''35$
			F814W	40	2	14	Saturated to $\sim 1''$
2B	$3.7 < V < 3.5$	2	F1042M	0.11	2	14	Minimally saturated
			F1042M	40	3	14	Saturated to $\sim 0\rlap{.}''5$
			F1042M	200	3	14	Saturated to $\sim 0\rlap{.}''75$
			F953N	40	3	14	Saturated to $\sim 0\rlap{.}''5$
			F814W	4	3	14	Saturated to $\sim 0\rlap{.}''75$
			F814W	40	3	14	Saturated to $\sim 1\rlap{.}''5$
3A	$0 < V < 1.3$	4	F1042M	0.11	1–2	14	Minimally saturated
			F1042M	14–40	3	14	Saturated to $0\rlap{.}''5–1''$
			F1042M	200	3	14	Saturated to $1\rlap{.}''25–2''$
			F953N	14–40	3	14	Saturated to $0\rlap{.}''5–1''$
			F953N	200	3	14	Saturated to $1\rlap{.}''25–2''$
3B	$V = -1.4$	1	F1042M	0.11	2	14	Minimally saturated
			F1042M	12	4	14	Saturated to $1''$
			F1042M	100	4	14	Saturated to $2''$
			F953N	12	4	14	Saturated to $1''$
			F953N	100	3	14	Saturated to $2''$

Gl 105A.—Four visits to this astrometric binary were executed. Results from the F814W and F555W images obtained in the first two visits were published shortly after the ground-based discovery of a VLM companion, Gl 105C (Golimowski et al. 1995a, 1995b). The final two visits to Gl 105AC were devoted to seeking fainter members of the system and to obtaining multiband photometry of Gl 105C. Thus, sets of three 0.3, 40, and 260 s exposures through F1042M were recorded during visits 3 and 4. Additional exposures through F336W (WFPC2 *U*), F439W (WFPC2 *B*), F675W, and F850LP (approximate Gunn *z*) were obtained for photometry of Gl 105C. The results pertaining to Gl 105C will be reported in another paper.

Gl 395 (36 Ursae Majoris A).—Two visits to this astrometric binary were executed. The first visit comprised short (1 and 35 s) exposures through F814W and F555W as an attempt to image the astrometric companion. During the second visit, sets of two or three 0.4, 8, and 200 s exposures were recorded through F1042M. Three 8 s exposures through F953N were obtained, and four exposures of 1 and 35 s were recorded through F814W. Because of Gl 395's relatively small proper motion ($0\rlap{.}''181 \, yr^{-1}$), no follow-up F1042M exposures were scheduled.

2.4. Faint-Companion Search Procedure

The first step toward identifying potential FCs in our target fields was to eliminate from consideration image artifacts and distant background objects. Cosmic-ray artifacts were eliminated by averaging like exposures with an algo-

rithm that rejects pixels deviating by at least 3 σ from the mean value at a given location. An optical artifact, or ghost image, resulting from an internal reflection in the PC's field-flattening lens (Krist 1995) was identified by its predictable location along the line connecting the PC's center and the target's image, its brightness relative to the target star (~ 1000 times fainter), and the similarity of its color to that of the target star. Background stars were easily identified after rotating, registering, and summing the corresponding pairs of exposures from different *HST* visits (Fig. 1). In the resultant images, the targets appeared as single point sources with two sets of pupil diffraction spikes separated angularly by the offset in *HST*'s roll angle between visits. All objects not sharing the proper motion of the target appeared double, with pairwise position angles opposite that of the target's proper and parallactic motion.

After identifying by eye the obvious artifacts and background objects in each field, a systematic search for FCs within the target's complicated PSF was performed. This step involved analyzing the cosmic-ray rejected and averaged F1042M and F814W images with the search algorithm described in detail in Paper I. (In brief summary, the search algorithm computes the Poisson noise, σ, for all contiguous 5×5 arrays of image pixels and identifies those 5×5 arrays containing at least four pixels with values exceeding a predetermined multiple of σ.) To make the search for all sources brighter than 10 σ tractable, sources were flagged in brightness decrements of 1 σ–10 σ, starting at 100 σ. As the search approached the 10 σ limit, smaller
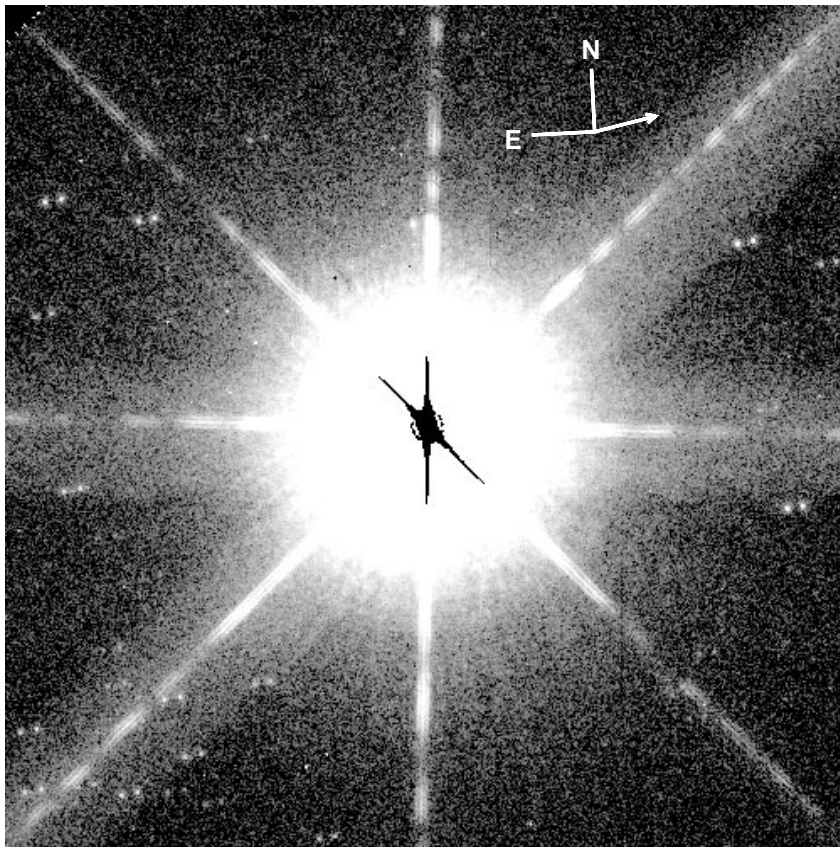
Fig. 1.—Sum of 400 s, F1042M images of Gl 551 (Proxima Centauri) recorded with the PC at two epochs separated by 21 days. The second-epoch image has been rotated and shifted so that the orientation and position of Gl 551 coincide with those of the first epoch. The field of view is $22\overset{''}{.}8 \times 22\overset{''}{.}8$, centered on the target. The roll offset between the two epochs is 44°, as evidenced by the angular separations of the two sets of pupil diffraction spikes and the two charge "bleeds" from the saturated images of the target (shown in black). The compass indicates the directions of north and east, while the arrow indicates the direction of Gl 551's proper motion. Note that all distant field sources appear double with a separation equal to 21 days of proper motion ($0\overset{''}{.}222$, or 4.8 PC pixels) and a position angle opposite to that of Gl 551's proper motion. Inspection of summed images such as this one permit immediate discrimination of brighter field sources from prospective FCs. Any FC would appear either as a single source or as a double source with a separation and position angle different from that expected for distant background sources.

decrements were used to offset the increasingly large number of flagged sources induced by high-frequency background variations of comparable amplitude near the core of the PSF. This growing influence of the target's PSF upon the search results at low thresholds rendered unlikely the prospect of a credible detection of a FC near a bright star.

During the search process, the $1'' \times 1''$ region around each flagged source was inspected using surface and contour plots to ascertain the nature of the source. In this manner, single-pixel defects ("hot pixels") were easily distinguished from images of stars or FCs, which typically span more than one pixel. Determining the relationship of a source to the larger scale structure of the target's PSF was often necessary, especially near the saturated core. The modulation of the Airy disk by diffraction from the mirror-support structures causes localized and regularly spaced enhancements of the PSF's diffraction rings. These local enhancements resemble beads on a string (see Fig. 1 of Golimowski & Schroeder 1998). A flagged "bead" could not be considered a FC candidate.

3. RESULTS

After several man months of searching the F1042M and F814W images of our target stars, no previously undetected FCs were found. Two known VLM companions, Gl 105C

(Golimowski et al. 1995a, 1995b) and GJ 1245C (McCarthy et al. 1988), were detected with very high S/N. Our images of the triple system GJ 1245ABC, discussed in § 3.3, are the first published direct images in which all three components are clearly resolved.

3.1. Faint-Companion Detection Limits

Because the brightnesses of our target stars differ greatly, no single exposure strategy could be adopted for our program. Consequently, the sensitivity of our program to FCs varied among the observing groups defined in § 2.2. Figures 2, 3, and 4 show the detection limits for the PC images of Gl 447 (Ross 128), Gl 144 (ϵ Eridani), and Gl 559A (α Centauri A), respectively, through the appropriate search bandpasses. These stars have V magnitudes that are average for the targets in groups 1, 2, and 3, respectively. Thus, the detection limits shown in Figures 2–4 are typical of those achieved for the targets in those respective groups.

The solid curves labeled "PSF" in Figures 2–4 are the azimuthally averaged, radial profiles of the targets' images obtained from the short- and long-exposure images through F1042M and F814W. The profiles were sampled over 5×5 pixel arrays in radial steps of $0\overset{''}{.}5$ and azimuthal intervals of 30°. Care was taken to avoid the diffraction spikes and the charge overflow from saturated pixels. The dashed curves
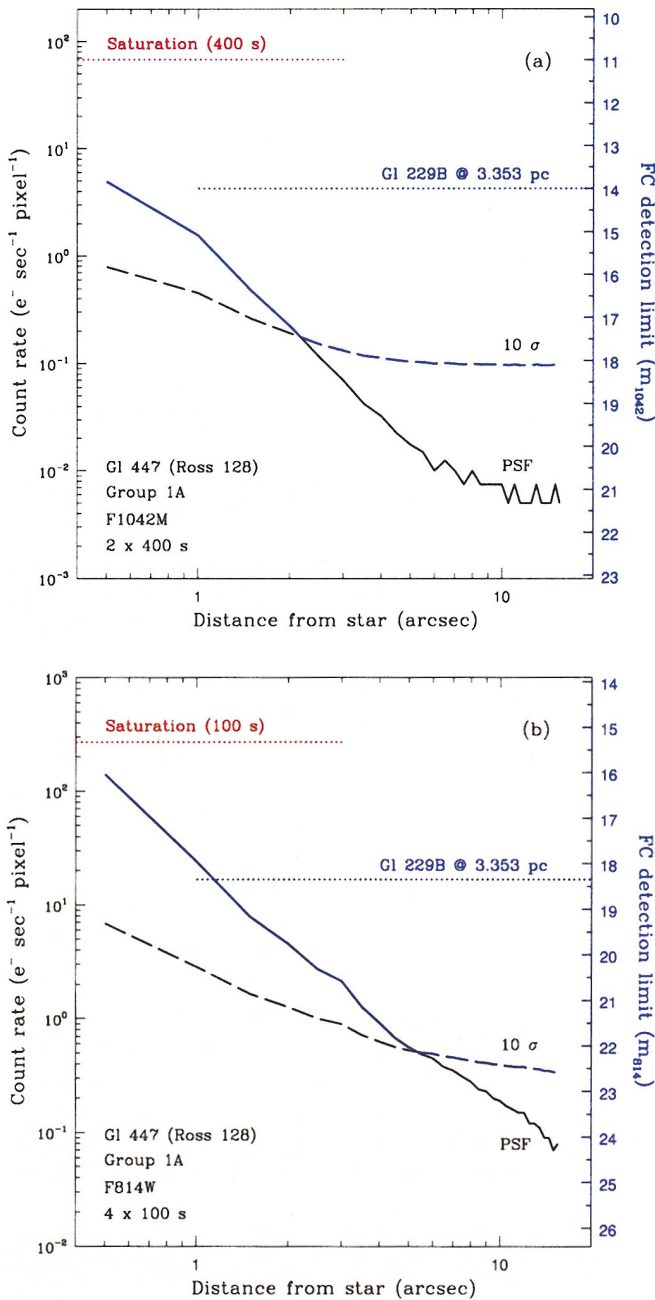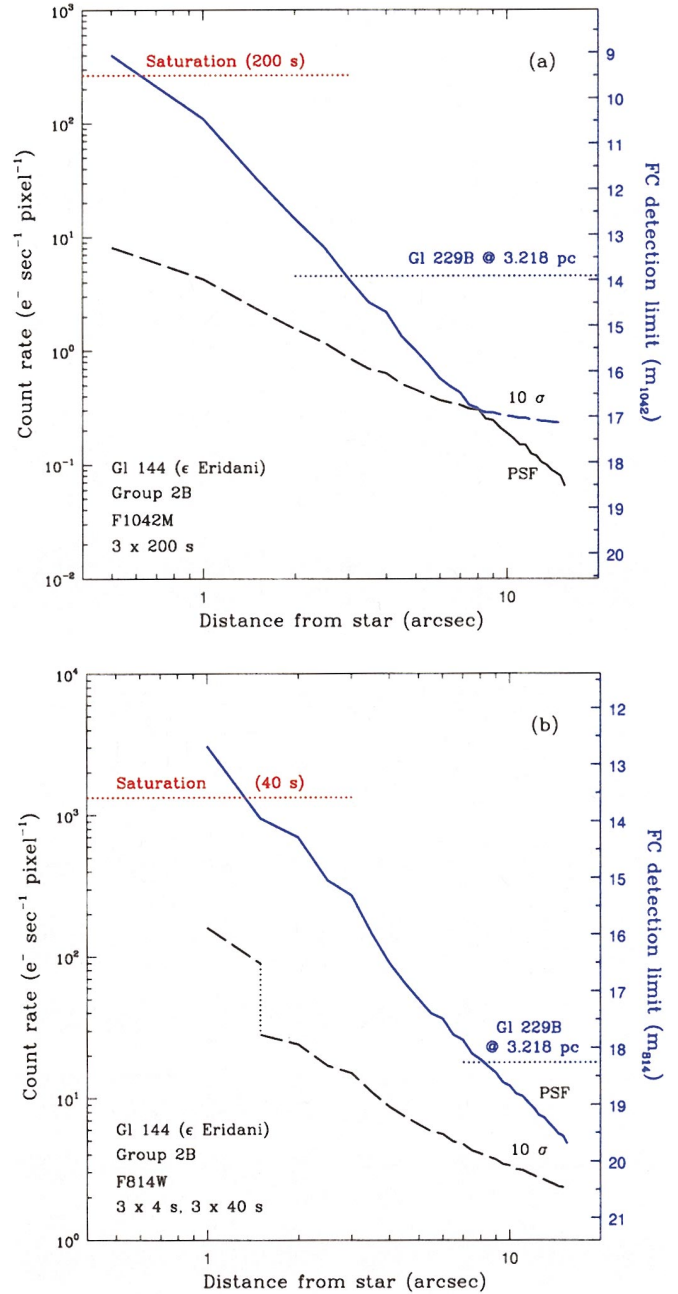
FIG. 2.—FC detection limits for PC images of Gl 447 (Ross 128) through (a) F1042M and (b) F814W. This star's V magnitude is average for the targets in group 1; the detection limits are therefore typical for group 1 targets. The solid curves labeled "PSF" are the azimuthally averaged, radial profiles of the target's images. The dashed curves labeled "10 σ" trace the signal level equal to 10 times the photon and read noise, combined in quadrature. The dotted red lines show the level of detector saturation for the longest exposure through each filter. Those portions of the PSF and 10 σ curves that mark the FC detection limit are shown in blue. See § 3.1 for an explanation of the detection-limit criteria. The dotted blue lines labeled "Gl 229B" reflect the apparent magnitudes of a Gl 229B–like brown dwarf projected to the distance of the target.

FIG. 3.—FC detection limits for PC images of Gl 144 (ε Eridani) through (a) F1042M and (b) F814W. This star's V magnitude is average for the targets in group 2; the detection limits are therefore typical for group 2 targets. All curves and symbols are as described in the legend to Fig. 2 and in § 3.1. The discontinuity in the F814W 10 σ curve at ~1″5 marks the transition between the shorter (4 s) and longer (40 s) exposure sets.

labeled "10 σ" trace the signal level equal to 10 times the photon and read noise, combined in quadrature. The dotted red lines show the levels of detector saturation for the longest exposures through each filter. The left (black) ordinate calibrates these curves as count rates in units of e^- s^{-1} pixel^{-1}. The right (blue) ordinate reflects the WFPC2 mag-

nitude of a point-source image whose central four pixels have the corresponding count rate.

Considering both S/N and image contrast, we now define our detection limit as the magnitude of a FC having four pixels equal to the larger of either the local value of 10 σ or the local brightness of the PSF. The former criterion is the same as defined in Paper I, but it is now valid only in those regions where the background variations are dominated by photon noise from the target's PSF or read noise. The latter criterion reflects the desire for an image contrast of at least 1 so that a FC may be readily distinguished from large and localized variations of the target's PSF. Those portions of
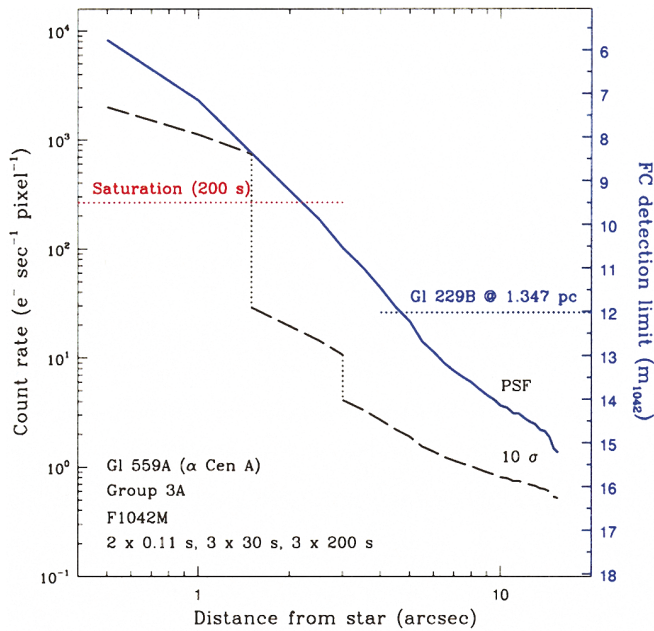
FIG. 4.—FC detection limits for PC images of Gl 559A (α Centauri A) through F1042M. This star's *V* magnitude is average for the targets in group 3; the detection limits are therefore typical for group 3 targets. All curves and symbols are as described in the legend to Fig. 2 and in § 3.1. The discontinuities in the 10 σ curve at ~1″.5 and 3″ mark the transitions between the 0.11, 30, and 200 s exposure sets.
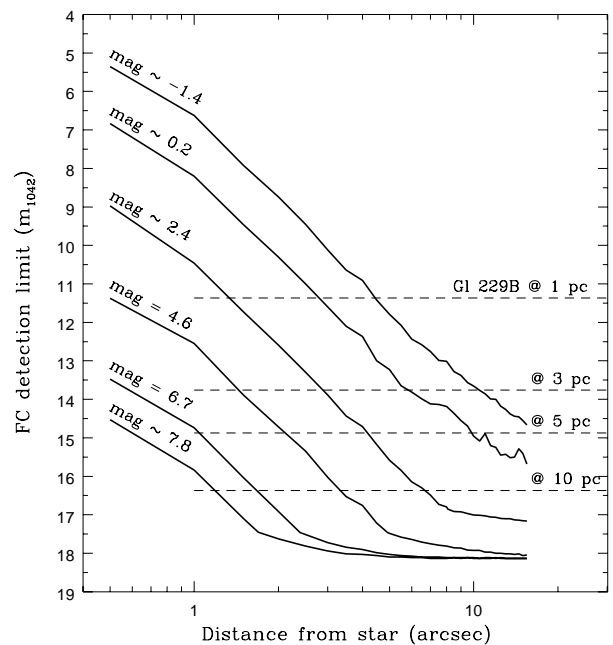
FIG. 5.—Summary of FC detection limits through F1042M for the range of apparent brightnesses spanned by the stars in our search. The curves are labeled with m_{1042} of the target stars for which the detection limits were measured. These stars are, from top to bottom, Gl 244A (Sirius), Gl 559B (α Centauri B), Gl 71 (τ Ceti), Gl 411 (Lalande 21185), Gl 729 (Ross 154), and Gl 406 (Wolf 359). The values of m_{1042} for Gl 411 and Gl 729 were obtained directly from unsaturated images of those stars. The values of m_{1042} for the remaining stars were estimated from ratios of the azimuthally averaged PSFs of these stars and other unsaturated stars. The dashed horizontal lines represent the apparent magnitudes of Gl 229B projected to distances of 1, 3, 5, and 10 pc.

the curves labeled "PSF" and "10 σ" that mark the FC detection limit for each target are shown in blue. For the faint group 1 targets (Fig. 2), the transitions between the contrast-limited and noise-limited FC detection thresholds occur at angular distances of 2″–5″ and 4″–14″ for F1042M and F814W, respectively. For the intermediate group 2 targets (Fig. 3), the transition occurs at 6″–8″ for F1042M; the transition for F814W occurs beyond the PC's field of view. For the bright group 3 targets (Fig. 4), the FC detection threshold is everywhere limited by the image contrast criterion. The shorter transition to noise-limited FC detection with F1042M exhibits one advantage of using F1042M as our primary search bandpass.

The dotted blue lines labeled "Gl 229B" in Figures 2–4 reflect the apparent F1042M and F814W magnitudes of a Gl 229B–like brown dwarf projected to the distance of the target. The gaps between these reference lines and the FC detection limits are greater for the F1042M images than for the F814W images at almost all separations, indicating that the older and lower mass ends of the substellar mass-age-luminosity relation can be probed more extensively with F1042M than with F814W (see § 4.1). This sensitivity to older and/or lower mass brown dwarfs demonstrates another advantage of searching for FCs through F1042M rather than through bluer, though more efficient, WFPC2 bandpasses. Figure 5 summarizes the FC detection limits through F1042M for the range of apparent brightnesses spanned by the stars in our sample.

To illustrate the detection limits more plainly, we show in Figure 6 sections of the deepest F1042M images of the representative stars from groups 1–3. To these image sections, we have added three sets of artificial FCs spaced by 1″ intervals and located 1″–14″ from each star. The artificial FCs were created from the PSF models described in Paper I and convolved with a 3 × 3–element kernel to simulate the

pixel-response function of the WFPC2 CCDs (Burrows et al. 1995). The labels to the right of each set identify the brightness of the constituent images as a factor of the integrated brightness of Gl 229B through F1042M (Golimowski et al. 1998). The brightnesses of the artificial FCs have been scaled to the distances of the respective target stars. Thus, each set of artificial FCs demonstrates the detectability of a FC having 0.01, 0.1, 1, or 10 times the F1042M luminosity of Gl 229B as a function of separation from the target star. Note that the artificial FCs labeled "1X" in Figure 6 are visible inward to distances matching those where the F1042M detection limits in Figures 2–4 equal the corresponding values of m_{1042} for a Gl 229B–like companion. The set of FCs marked "0.01X" in Figure 6a represents objects that are 1 mag fainter than the ultimate 10 σ detection limit for the 400 s exposures through F1042M (see Fig. 2a).

3.2. *Photometry in the F1042M Bandpass*

Short (≤40 s) and long (100–400 s) exposures of the target stars were recorded through F1042M to allow unsaturated or minimally saturated images of even the brightest stars. Consequently, m_{1042} (the apparent magnitude through F1042M) could be measured or estimated for all the targets and their companions. To ensure accurate photometry, the data were recalibrated using the reference files recommended for those data by the Space Telescope Science Institute Data Archive on 1999 June 8. When appropriate, the recalibrated images were scaled to correct for the 0.125 or 0.250 s exposure-time errors caused by the
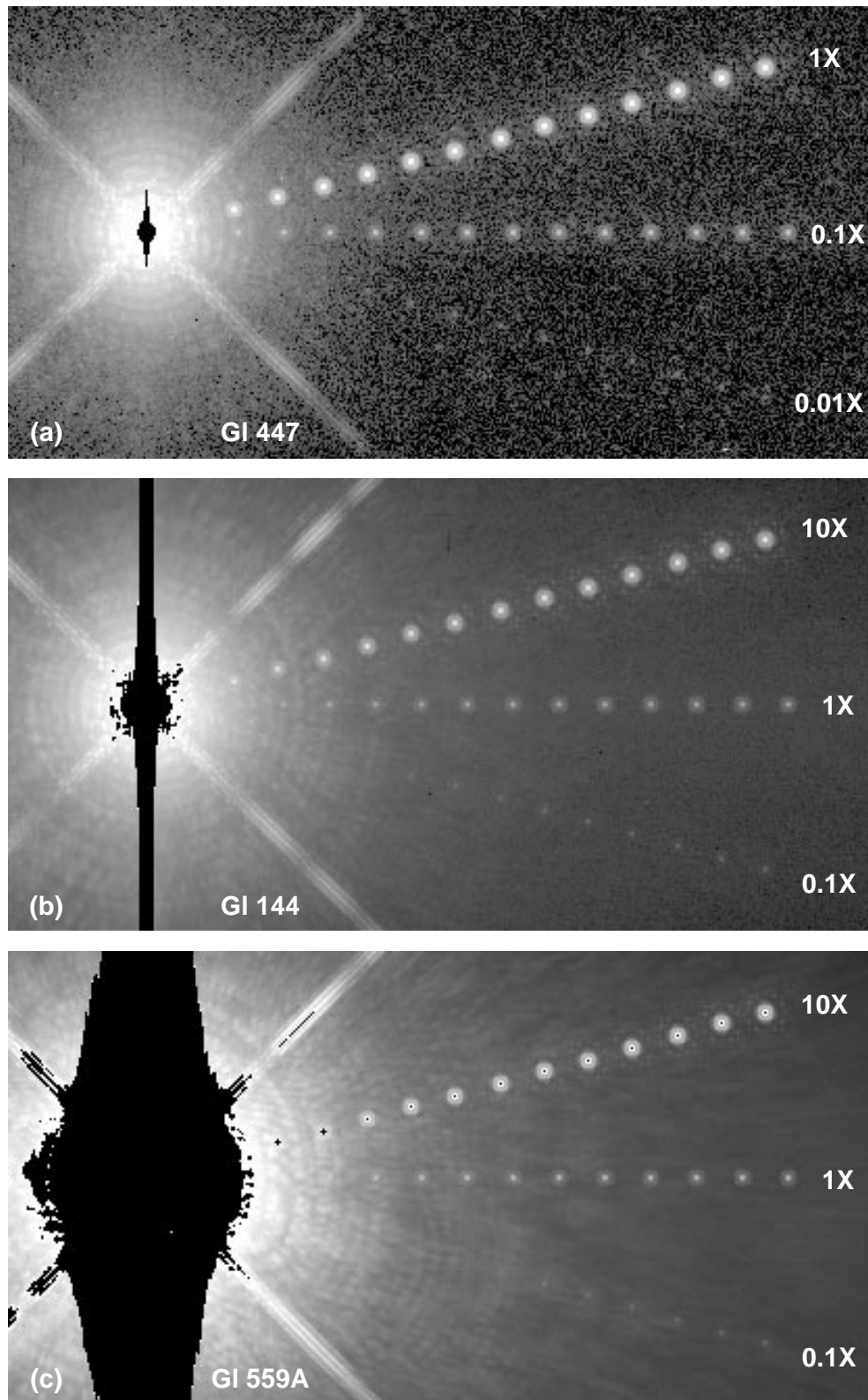
FIG. 6.—19″ × 10″ sections of the deepest F1042M images of the representative stars from groups 1–3. Saturated pixels are blackened. Three sets of artificial FCs spaced by 1″ intervals and located 1″–14″ from each star have been added to each image. The labels to the right of each set identify the brightness of the constituent images as a factor of the integrated brightness of Gl 229B through F1042M. The brightnesses of the artificial FCs have been scaled to the distances of the respective target stars. Thus, each set of artificial FCs demonstrates the detectability of a FC having 0.01, 0.1, 1, or 10 times the F1042M luminosity of Gl 229B as a function of separation from the target star. (a) Demonstration of detection limits for group 1 target Gl 447 (Ross 128). The set of FCs marked "0.01X" represents objects that are 1 mag fainter than the ultimate 10 σ detection limit for the 400 s exposures through F1042M (see Fig. 2a). (b) Demonstration of detection limits for group 2 target Gl 144 (ϵ Eridani). (c) Demonstration of detection limits for group 3 target Gl 559A (α Centauri A). Note that the artificial FCs marked "10X" saturate the detector in 200 s.

concurrent activation of the WFPC2 shutter blades and serial clocks (Baggett 1995).[6]

For unsaturated images of single or widely separated multiple targets, we measured m_{1042} using the technique of Holtzman et al. (1995a) for point-source photometry. For closely separated multiples, we obtained m_{1042} by fitting appropriately scaled and registered PSF models generated by the Tiny Tim software package (Krist & Hook 1997) for each component. Because the actual F1042M PSFs exhibit wide-angle scattered light exceeding that expected from diffraction alone, we added to the standard Tiny Tim models an azimuthally symmetric scattered-light halo that closely matches the observed excess (Krist 2000). Photometry of single-star images having four or fewer saturated pixels was also obtained using the improved Tiny Tim models. For heavily saturated images that showed charge overflow, we derived m_{1042} by comparing the unsaturated and azimuthally averaged regions of the targets' PSFs with those of comparably exposed stars for which unsaturated images were also obtained.

We did not correct the measured signals for possible losses from degraded charge-transfer efficiency (CTE). Instead, we included in our photometric error estimate a 2% uncertainty attributed to CTE loss in accordance with the recommendation of Holtzman et al. (1995a) for images located at the center of the detector. We also included in our estimated error a 1% uncertainty attributed to local flat-field variations and a 2% uncertainty of the synthetic zero point for F1042M (Holtzman et al. 1995a). To the model-based photometry, we added a 2% uncertainty that reflects the dispersion between the model-based and standard aperture photometry of several unsaturated reference images. Together, these instrumental and modeling effects dominated statistical noise and background-subtraction error in the resultant photometric uncertainties.

The measured values of m_{1042} and their corresponding uncertainties for each target are listed in Table 3. Figure 7 shows a color-magnitude diagram constructed from these values and the values of V and d listed in Table 1 for each target. The regions of this diagram occupied by white dwarfs and main-sequence stars of different spectral types are marked. Data representing targets with spectral types later than M5 are also labeled for ease of identification. As we explain in § 3.3, the end of the hydrogen-burning main sequence occurs at $M_{1042} \approx 12$. Thus, a star with the minimum main-sequence mass of 0.08 $M_\odot$ located at distances of 1, 3, 5, and 10 pc would be 11.0, 8.6, 7.5, and 6.0 mag brighter than the ultimate detection limit of our search through F1042M (see Fig. 2a). Such photometric depth makes our search for FCs to nearby stars the most sensitive yet published. We discuss how this photometric sensitivity transforms into the detectability of substellar companions in § 4.1.

3.3. The Triple System GJ 1245ABC

The astrometric binary GJ 1245AC was first resolved by McCarthy et al. (1988) using one-dimensional speckle interferometry. With a mass of 0.074 ± 0.013 $M_\odot$, GJ 1245C is the least massive object outside the solar system for which a mass has been derived from dynamical elements (Henry et
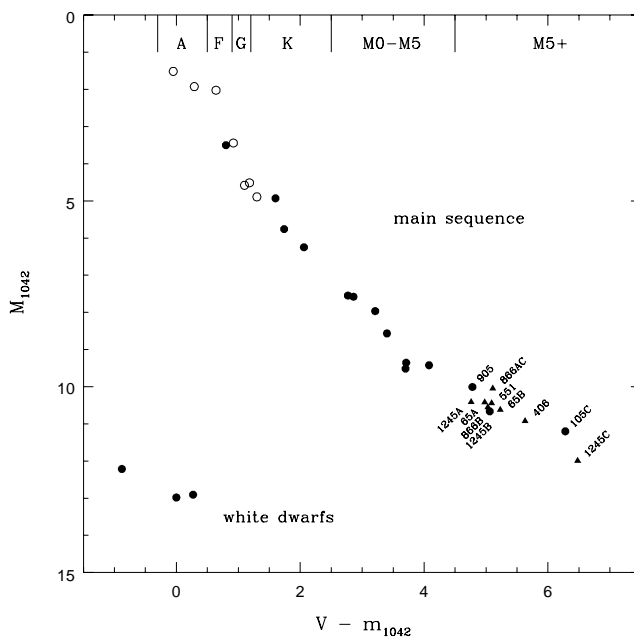

FIG. 7.—Color-magnitude diagram of all program targets and their companions. Values of m_{1042} were obtained by using the technique of Holtzman et al. (1995a) for WFPC2 point-source photometry (filled circles), by comparing unsaturated regions of the targets' PSFs with those of comparably exposed stars for which aperture photometry was obtained (open circles), or by fitting appropriately scaled and registered binary-PSF models generated by Tiny Tim (triangles). The colors and absolute magnitudes were computed using values of V and d from Table 1. The uncertainties of these data are listed in Table 3 and are smaller than the plotted symbols. The data for targets with spectral types later than M5 V are labeled by their CNS3 numbers (Gl or GJ).

al. 1999). The derived mass firmly places GJ 1245C in the theoretical transition region between stars and brown dwarfs (Burrows et al. 1993). Thus, the absolute F1042M magnitude listed in Table 3 for GJ 1245C establishes the observational end of the main sequence at $M_{1042} \approx 12$. The position of GJ 1245C in Figure 7 suggests for that object a spectral type later than M6 or M7, which have been derived for Gl 105C by Rudy, Rossano, & Puetter (1996) and Golimowski et al. (1995b), respectively.

Figure 8 shows the average of three 40 s F1042M images of GJ 1245ABC recorded on UT 1997 October 12. To our knowledge, Figure 8 is the first published direct image in which all three components of the system are resolved. The positions of the stars were determined from the centroids of either the actual F1042M images (GJ 1245B) or the Tiny Tim models best fitting the data (GJ 1245A and GJ 1245C). These centroids were corrected for field distortion using the Space Telescope Data Analysis System task METRIC. (All positions hereafter appearing in this paper have been corrected likewise.) Because the signal-to-noise ratios of the components' images are high, the uncertainties in the centroids are dominated by the accuracy of the centroid algorithm and the rms error of the distortion correction. Combining these uncertainties, we estimate a centroid error of ~0.16 pixel (Golimowski et al. 1998). We obtain an absolute position-angle uncertainty of 0°07 from the nominal guide-star position error of 1″. The separations and position angles of GJ 1245B and GJ 1245C relative to GJ 1245A at each epoch, assuming an image scale of 0″.04554 pixel^{-1} (Holtzman et al. 1995b), are presented in Table 4.

---

[6] See the World Wide Web page http://www.stsci.edu/instruments/wfpc2/Wfpc2_stan/1995/wpstan3.html.

TABLE 3

F1042M Photometry of Program Stars

CNS3 Name	m_{1042}	M_{1042}	Method[a]
Gl 15A	5.31 ± 0.03	7.55 ± 0.04	Apphot
Gl 65A	7.56 ± 0.05	10.43 ± 0.06	Model
Gl 65B	7.77 ± 0.05	10.63 ± 0.06	Model
Gl 71	2.39 ± 0.04	4.58 ± 0.04	Ratio
Gl 105A	4.22 ± 0.03	4.93 ± 0.05	Apphot
Gl 105C	10.49 ± 0.03	11.20 ± 0.05	Apphot
Gl 144	2.43 ± 0.04	4.89 ± 0.04	Ratio
Gl 244A	-1.38 ± 0.04	1.52 ± 0.04	Ratio
Gl 244B	9.32 ± 0.04	12.22 ± 0.04	Apphot
Gl 280A	-0.26 ± 0.04	2.02 ± 0.04	Ratio
Gl 280B	10.70 ± 0.05	12.98 ± 0.06	Apphot
Gl 395	4.04 ± 0.03	3.50 ± 0.05	Apphot
Gl 406	7.82 ± 0.05	10.93 ± 0.06	Model
Gl 411	4.61 ± 0.03	7.58 ± 0.04	Apphot
Gl 440	11.23 ± 0.03	12.90 ± 0.05	Apphot
Gl 447	7.05 ± 0.03	9.43 ± 0.05	Apphot
Gl 551	6.00 ± 0.05	10.44 ± 0.05	Model
Gl 559A	-0.91 ± 0.05	3.44 ± 0.05	Ratio
Gl 559B	0.16 ± 0.04	4.52 ± 0.04	Ratio
Gl 669	5.83 ± 0.03	9.52 ± 0.04	Apphot
Gl 725A	5.69 ± 0.03	7.97 ± 0.05	Apphot
Gl 725B	6.29 ± 0.03	8.56 ± 0.05	Apphot
Gl 729	6.72 ± 0.03	9.36 ± 0.04	Apphot
Gl 768	0.48 ± 0.04	1.92 ± 0.04	Ratio
Gl 820A	3.47 ± 0.03	5.76 ± 0.04	Apphot
Gl 820B	3.97 ± 0.03	6.25 ± 0.04	Apphot
Gl 866AC	7.74 ± 0.05	10.05 ± 0.08	Model
Gl 866B	8.24 ± 0.05	10.55 ± 0.08	Model
Gl 905	7.51 ± 0.03	10.01 ± 0.04	Apphot
GJ 1245A	8.70 ± 0.05	10.41 ± 0.06	Model
GJ 1245B	8.95 ± 0.03	10.66 ± 0.04	Apphot
GJ 1245C	10.28 ± 0.05	11.99 ± 0.06	Model

[a] Apphot, aperture photometry of Holtzman et al. 1995a; Model, Tiny Tim PSF model fit; Ratio, ratio of azimuthally averaged PSFs. The photometric zero point used for all methods is adopted from Holtzman et al. 1995a.

Figure 9 shows the observed positions of GS 1245AC together with the positions expected for the same observational epochs using the photocentric-orbit elements reported by Harrington (1990). We transformed these photocentric elements into the orbital elements of GJ 1245C relative to GJ 1245A using the latest derived masses for each component (Henry et al. 1999). Although our measured positions lie close to the orbital ellipse, they lag the expected positions by ~ 18 months. The uncertainties of both our measured positions ($\pm 0''.01$–$0''.02$ in each coordinate) and the published orbital elements are too small to reconcile this large discrepancy in phase. However, our measured positions agree very well with the positions measured over the last three years with *HST*'s Fine Guidance Sensors (FGS) as part of an interferometric program to define the lower end of the stellar mass-luminosity relation (MLR; T. Henry 1999, private communication). The agreement between the WFPC2 and FGS measurements indicates that at least one of the orbital elements of Harrington (1990)—perhaps the time of periastron passage—is incorrect.

The images of all three components of GJ 1245ABC were heavily saturated in the F675W and F814W images recorded during both *HST* visits. Nevertheless, we estimated the apparent magnitudes in each bandpass by fitting model PSFs generated with Tiny Tim to the unsaturated regions

TABLE 4

Separations and Position Angles of Multiple Systems

CNS3 Name	UT	Separation (arcsec)	P.A. (deg)
Gl 65AB	1997 Jun 26	0.796 ± 0.007	294.68 ± 0.85
	1997 Jul 27	0.749 ± 0.007	290.62 ± 0.83
Gl 244AB	1997 Mar 19	3.691 ± 0.011	192.64 ± 0.30
	1997 May 18	3.711 ± 0.009	189.76 ± 0.25
Gl 280AB	1997 Mar 12	4.743 ± 0.009	53.69 ± 0.19
	1997 May 17	4.734 ± 0.009	54.71 ± 0.17
Gl 866AC-B	1997 Jun 26	0.488 ± 0.007	345.75 ± 1.71
	1997 Jul 27	0.486 ± 0.007	343.79 ± 1.72
GJ 1245AB	1997 Jun 25	7.066 ± 0.007	82.67 ± 0.12
	1997 Oct 12	7.031 ± 0.007	82.59 ± 0.14
GJ 1245AC	1997 Jun 25	0.609 ± 0.007	304.27 ± 1.34
	1997 Oct 12	0.604 ± 0.007	296.44 ± 1.27

of the components' images. Given the loss of data in the image cores, these fits are probably accurate to 10%. The estimated magnitudes and uncertainties for GJ 1245ABC in the three survey bandpasses are shown in Table 5.

3.4. Results for Other Targets

We now present additional results and notes for individual targets, listed in order of their appearance in Table 1.

Gl 551 (Proxima Centauri).—Sections of the 10 and 40 s F1042M images of Gl 551 were presented previously by Golimowski & Schroeder (1998). These images dispute the reported detection by Schultz et al. (1998b) of a possible substellar companion located $\sim 0''.3$ from Gl 551. Moreover, we find no evidence for a VLM companion in our deep F1042M images to the limits exhibited in Figure 5 for a $m_{1042} \approx 6$ target.

Gl 699 (Barnard's Star).—The possibility of a planetary system around Gl 699 has been much studied and debated (van de Kamp 1986; Gatewood 1995; Benedict et al. 1999). Current *HST* astrometry puts upper limits on the masses of any planets at a few tenths of a Jupiter mass (M_J) for orbital periods longer than 150 days and radii greater than 0.3 AU ($0''.16$). Our search is insensitive to gaseous planets of such mass and angular separation unless they are aged less than $\sim 10^7$–10^8 yr (Burrows et al. 1997). As the star's large space motion is consistent with an old-disk or halo population (Leggett 1992), this model-based constraint is not illuminating.

Gl 411 (Lalande 21185).—Gatewood (1996) has reported astrometric perturbations of Gl 411 that may be caused by as many as three planetary bodies, one of which is located at separations greater than $0''.8$. As in the case of Gl 699 (Barnard's Star), our search for companions to Gl 411 does not significantly constrain the nature of these planets or the likelihood of their existence. Our null result eliminates only the possibility that the long-period astrometric perturbation is caused by a Jupiter- or Saturn-sized planet aged less than $\sim 10^7$ yr (Burrows et al. 1997). Again, the star's large space motion (Leggett 1992) renders this conclusion academic.

Gl 244AB.—The possible triplicity of Sirius has been discussed and debated for over 100 years. Recently, Benest & Duvent (1995) performed numerical simulations of the hypothetical triple system and determined that stable orbits with a 6 yr period can exist for a Sirius C around Sirius A. No orbits with periods greater than 4 yr can stably exist

TABLE 5

THREE-BAND WFPC2 PHOTOMETRY OF GJ 1245ABC

COMPONENT	F675W		F814W		F1042M	
	m	M	m	M	m	M
A	$11.86^{+0.11}_{-0.12}$	$13.57^{+0.12}_{-0.13}$	$10.05^{+0.11}_{-0.12}$	$11.77^{+0.12}_{-0.13}$	8.70 ± 0.05	10.41 ± 0.06
B............	$12.31^{+0.11}_{-0.12}$	$14.02^{+0.12}_{-0.13}$	$10.37^{+0.11}_{-0.12}$	$12.08^{+0.12}_{-0.13}$	8.95 ± 0.03	10.66 ± 0.04
C	$14.92^{+0.11}_{-0.12}$	$16.63^{+0.12}_{-0.13}$	$12.03^{+0.11}_{-0.12}$	$13.75^{+0.12}_{-0.13}$	10.28 ± 0.05	11.99 ± 0.06

about Sirius B. The authors also concluded that Sirius C, if it exists, has a mass no greater than 0.05 $M_{\odot}$ and may be separated by up to 3″ from Sirius A. Our observations of Sirius reveal no such companion, but they do not exclude its existence. More observations over a 6 yr period are needed to constrain the possibility of a third component.

Because our images of Sirius were heavily saturated, we inferred the star's location by repeatedly marking the midline of the diffraction spikes from the secondary-mirror support and then computing the intersection of the orthogonal pairs of spikes. This technique rendered the star's position to an accuracy of ±0.2 pixel. We determined the position of Sirius B from its image centroid after subtrac-

tion of a bivariate polynomial fit to the local background. The measured separations and position angles of Sirius B at each epoch are presented in Table 4. Figure 10 shows these measured positions together with those predicted from the orbital elements computed by Benest & Duvent (1995) for each epoch. The observed positions of Sirius B fall directly on the computed orbit, but lag by ∼75 days the expected positions for those epochs. Benest & Duvent (1995) did not assign uncertainties to their orbital elements, so we cannot assess the significance of this discrepancy. Note, however, that our observations occurred almost exactly at periastron, i.e., where the orbital velocities are greatest and the predicted positions are usually most uncertain.
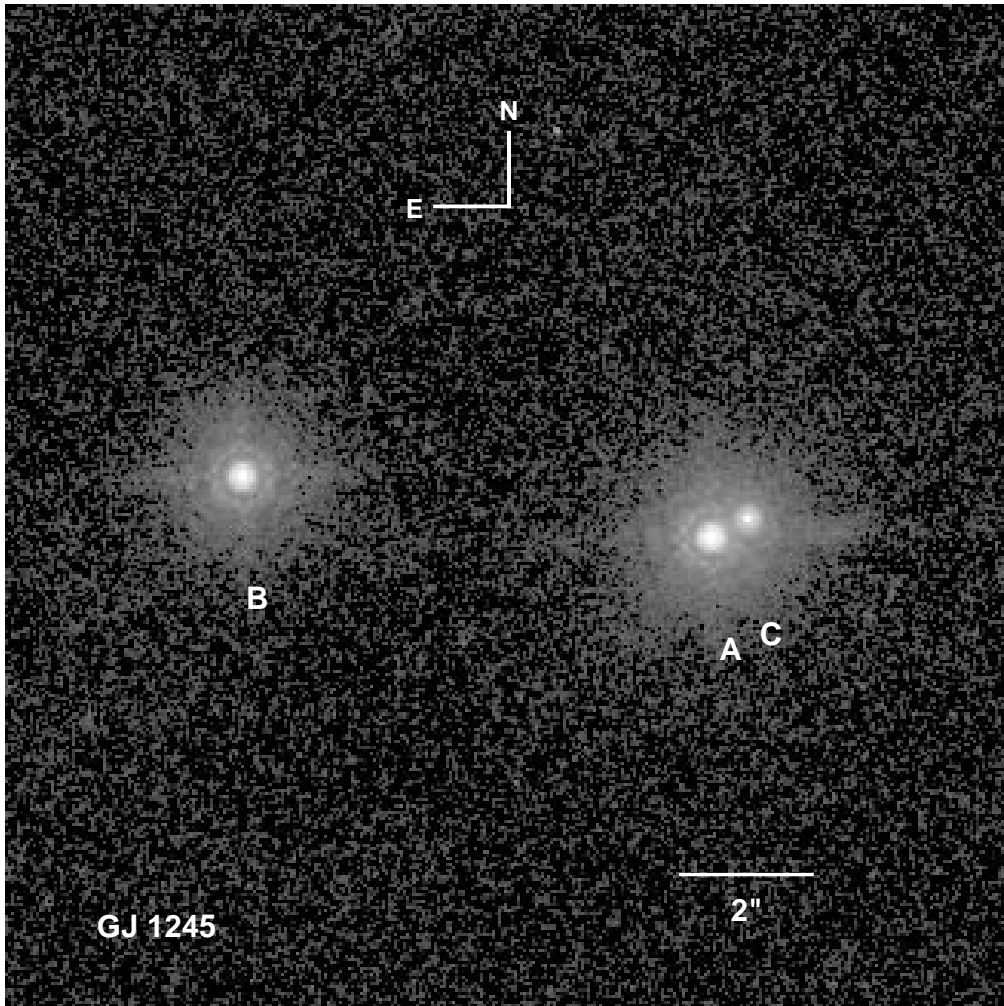

FIG. 8.—PC image of GJ 1245ABC through F1042M recorded on UT 1997 October 12. The field of view is 15″ × 15″. The logarithm of the image is displayed to reduce dynamic range. This view is the first published direct image in which all three components of the system are resolved.
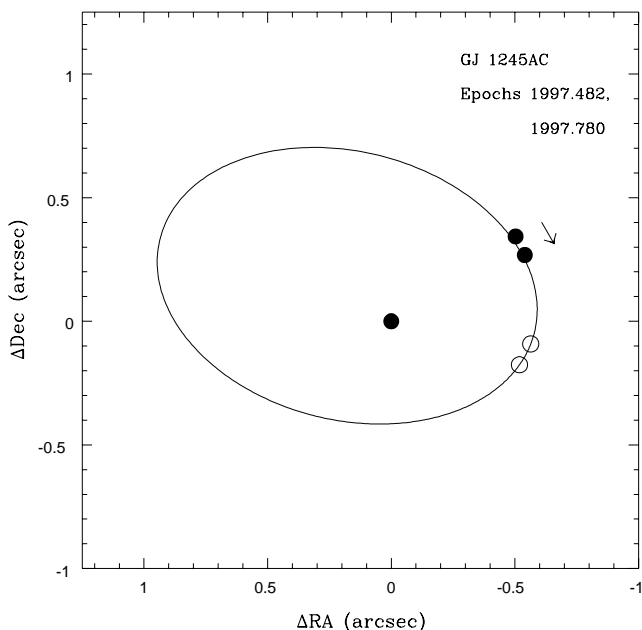
FIG. 9.—Comparison of observed positions of GJ 1245AC with positions expected from orbital elements of Harrington (1990) for the same epochs of observation. Filled circles represent the observed locations of the components. The primary star, GJ 1245A, is located at the origin of the coordinates. Open circles represent the positions computed from the orbital elements. The uncertainties of our positions are ±0″.01–0″.02 in each coordinate, i.e., much smaller than the radii of the filled circles. The ellipse traces the published orbit of GJ 1245C relative to GJ 1245A. The arrow represents the direction of motion.

Gl 65AB.—The observed relative positions of this much-studied low-mass binary are presented in Table 4. The uncertainties of separation and position angle correspond to an uncertainty of ∼0″.012 in both right ascension and declination. As Figure 10 shows, these uncertainties are 3–5 times smaller than the discrepancies between our measured positions and those predicted from the orbital elements of Geyer, Harrington, & Worley (1988) for each epoch. If we crudely ascribe these discrepancies to an underestimate of the orbit's semimajor axis, then the masses of the components will be larger than those derived by Geyer et al. (1988) by an amount equal to the ratio of the observed and expected semimajor axes (∼1.14). In such a case, we estimate the masses of Gl 65A and Gl 65B to be 0.115 $M_\odot$ and 0.113 $M_\odot$, respectively.

Gl 866ABC.—Gl 866 is a triple-lined spectroscopic system (Reid & Gizis 1997a; Delfosse et al. 1999). The closer pair, Gl 866AC, has not been resolved by direct imagery or speckle interferometry. The observed relative positions of the visual components AC and B are presented in Table 4. Figure 10 shows our measured positions and the positions expected from the orbital elements of Leinert et al. (1990) for each epoch. The observed positions of Gl 866B lie squarely on the computed relative orbit, but they lag the expected positions by ∼100 days. This lag greatly exceeds the ±12 days uncertainty in the date of periastron passage computed by Leinert et al. (1990). More observations are required to investigate fully the accuracy of the computed orbital elements.

Gl 820AB.—This wide binary star was imaged with its barycenter positioned near the center of the PC. Thus, the field of search for FCs was not symmetric about each star. The average separation and position angle of this slowly

moving pair between UT 1997 March 26 and UT 1998 August 15 were 30″.44 ± 0″.04 and 149°.49 ± 0°.09, respectively.

Gl 280AB.—Because our images of Procyon were heavily saturated, we inferred the star's location by repeatedly marking the midline of the diffraction spikes from the secondary-mirror support and then computing the intersection of the orthogonal pairs of spikes. This technique rendered the star's position to an accuracy of ±0.2 pixel. We determined the position of Procyon B from its image centroid after subtraction of a bivariate polynomial fit to the local background. The measured separations and position angles of Procyon B at each epoch are presented in Table 4. We compare graphically these observed positions with those predicted from the orbital elements of Irwin et al. (1992) in Figure 10. The discrepancies between the observed and predicted positions greatly exceed our astrometric uncertainty of ∼0″.018 for each celestial coordinate. The observed positions lag the predicted positions by ∼10°, which, for our epochs of observation, corresponds to a time lag of ∼600 days. The expected separation of Gl 280AB at a position angle of 53°.7 is 5″.01, i.e., 0″.27 larger than the separation observed on UT 1997 March 12. This discrepancy supports the proposition of Irwin et al. (1992) that an overestimate by ∼0″.2 of the predicted separation would lower the computed mass of Procyon sufficiently to resolve the long-standing inconsistency between its observed luminosity and that derived from the theoretical MLR. Bond et al. (1999) reported the same result based on their WFPC2 images of Procyon recorded throught the ultraviolet filter F218W.

Gl 725AB.—This wide binary star was imaged with its barycenter positioned near the center of the PC. Thus, the field of search for FCs was not symmetric about each star. The average separation and position angle of this pair between UT 1997 June 26 and UT 1997 August 2 were 12″.861 ± 0″.005 and 172°.72 ± 0°.06, respectively.

Gl 15AB.—Because this binary star has a separation of ∼41″, it was impractical to place both stars on the PC. During each visit, Gl 15A was acquired at the center of the PC. A spacecraft roll angle of 277° during the first visit on UT 1997 May 25 forced the placement of Gl 15B in the quadrant of the Wide Field Camera 2 (WF2) nearest the output node. Thus, the field of search was symmetric about Gl 15A, while that about Gl 15B was asymmetric with a wider field of view. A spacecraft roll angle of 257° during the second visit on UT 1997 June 18 unfortunately placed Gl 15B in a region within WF2 that is vignetted by the shadow of the WFPC2 pyramid (Burrows et al. 1995). Because the shortest WF2 exposures through F1042M were not recorded, no unsaturated image of Gl 15B was obtained. Consequently, Gl 15B has been omitted from Table 3.

Gl 105AC.—Golimowski et al. (1995b) first imaged the VLM star Gl 105C at an angular distance of ∼3″.3 from the astrometric binary Gl 105A. The WFPC2 *V* and *I* magnitudes of Gl 105C are consistent with an M7 spectral type (Golimowski et al. 1995a). Although its mass is consistent with astrometric estimates, Gl 105C is observed at approximately 3 times the angular separation predicted from two independent, albeit disparate, astrometric studies (Ianna 1992; Heintz & Cantor 1994). The large discrepancy between the period of the astrometric perturbation (∼60 yr) and the probable period of Gl 105AC's orbit (≳150 yr) raises speculation that another, previously unseen, compan-
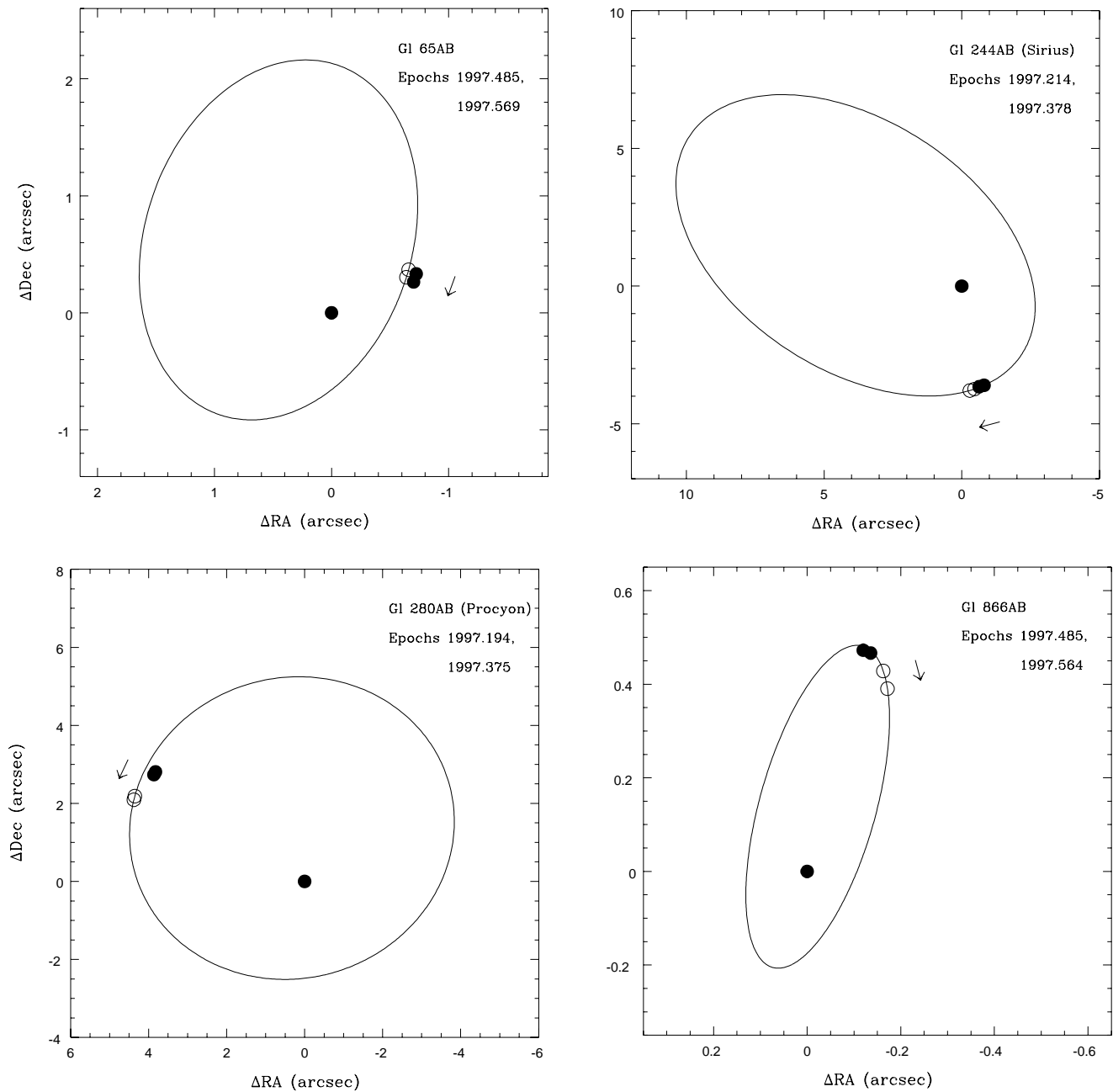
Fig. 10.—Comparison of observed positions of four visual binaries with positions expected from published orbital elements for the same epochs of observation. All symbols and uncertainties are as described in the legend to Fig. 9. See text for comments and references.

ion is the perturbing agent. No such companion was detected, however, in any of the F1042M images of Gl 105A obtained on UT 1997 December 6 and UT 1998 January 4, to limits approximated by the $m_{1042} = 4.6$ curve in Figure 5. An M7 companion like Gl 105C ($m_{1042} = 10.5$) would have been detected beyond $\sim 0\rlap{.}''3$ from Gl 105A, and a Gl 229B–like companion would have been detected at separations $\gtrsim 3''$. Unless its orbital phase placed it fortuitously within $0\rlap{.}''3$ of Gl 105A, an astrometric companion with an expected mass of $\gtrsim 0.08\ M_\odot$ would have been detected easily by us. The nature of Gl 105C and its possible role as the astrometric companion will be described in another paper.

   Gl 395 (36 Ursae Majoris A).—Lippincott (1983) reported an astrometric perturbation of Gl 395 consistent with a 70 M_J

companion in a 18 yr orbit. Campbell, Walker, & Yang (1988) discounted this companion after they failed to detect a radial acceleration consistent with the astrometric orbital phase for their observational epoch. Nelson & Angel (1998) noted a long-term trend in the radial-velocity data of Walker et al. (1995) that is consistent with either a planet of mass 2 M_J in a 10 yr orbit or a brown dwarf of mass 20–30 M_J in a 50 yr orbit. As Figure 5 indicates, our survey would have detected a Gl 229B–like brown dwarf beyond $\sim 5''$ from Gl 395. Thus, our nondetection does not exclude either companion suggested by Nelson & Angel. Lippincott's astrometric companion would have been within one year of periastron (i.e., $\sim 0\rlap{.}''1$ separation) at the time of our F1042M observation (UT 1997 March 25) and therefore undetectable with the PC.

4. DISCUSSION

4.1. *Physical Interpretation of Detection Limits*

To place the null result of our search for FCs to nearby stars in an astronomical context, we must convert the photometric limits of our search into constraints on the masses of any undetected companions. This task requires the use of MLRs for the bandpasses of our search. While the MLRs for VLM stars observed through F1042M and F814W can be uniquely derived via direct observation of known VLM stars or synthetic photometry, the MLRs for substellar objects cannot. Because brown dwarfs cool with age, their temperatures and luminosities (i.e., their colors and magnitudes) vary with both mass and time. No empirical mass-age-luminosity relation for brown dwarfs yet exists, so we must rely on theoretical models to interpret our observational limits as physical constraints. Although brown dwarf models have typically failed to reproduce adequately the optical spectrum of Gl 229B, recent models that consider the effects of warm dust and extreme pressure deep in the brown dwarf's photosphere have produced very encouraging results (Tsuji, Ohnaka, & Aoki 1999).

We first assess our search's sensitivity to VLM stellar companions around our target stars. Figure 7 indicates that the empirical end of the main sequence (mass of $\approx 0.08\ M_\odot$) occurs at $M_{1042} \approx 12$. According to Figure 5, we would have detected within the entire PC field any stellar companions to those targets lying within 5 pc and having brightnesses $m_{1042} \gtrsim 4$. These distance and brightness limits include all our group 1 and faint ($V > 6$) group 4 targets (see Table 1). Moreover, we would have detected any stellar companions separated by $\gtrsim 0\rlap{.}''5$ from all the group 2 targets and Gl 105A, as well as any stellar companions separated by $\gtrsim 1''$ from all the group 3 targets and Gl 395. In short, only the lowest mass stellar companions lying within $0\rlap{.}''5$ to $1''$ of our brightest targets would have escaped our notice.

To date, the most comprehensive published models of brown dwarf atmospheres, spectra, and evolution are those of Burrows et al. (1997). Convolving their model spectra with the standard J, H, and K bandpasses, the authors showed in several types of near-infrared color-magnitude diagrams the isochrones of brown dwarfs with $T_{\rm eff} < 1300\ {\rm K}$. Although Burrows et al. (1997) produced no optical color-magnitude diagrams with such isochrones, we may, with a few reasonable assumptions, translate their near-infrared results into a form useful for our F1042M search. Inspecting the evolution of the model brown dwarf spectra over a wide range of masses (0.001–$0.020\ M_\odot$) and ages (0.1–5.0 Gyr), we note that the fluxes in the F1042M and J bandpasses maintain nearly constant proportion (see Figs. 15–19 of Burrows et al. 1997). Thus, the $m_{1042} - J$ color of these model spectra remain roughly constant within these ranges of mass and age. Assuming this to be true, we may use the $m_{1042} - J = 1.0$ obtained for Gl 229B (Matthews et al. 1996; Golimowski et al. 1998) to correlate our F1042M detection limits with the theoretical J-band isochrones of cool brown dwarfs.

Employing the above assumptions, we show in Figures 11–13 the theoretical detection limits of our search for brown dwarfs aged 0.5, 1.0, and 5.0 Gyr, respectively. Each figure shows the same photometric detection limits (black curves) shown in Figure 5 for targets of various brightnesses. The horizontal lines reflect the apparent F1042M
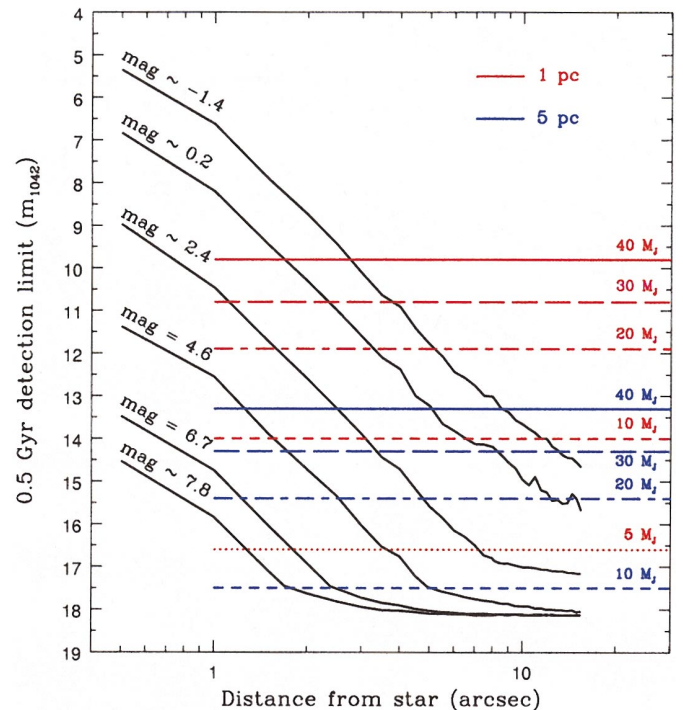

Fig. 11.—Theoretical limits of sensitivity to brown dwarfs aged 0.5 Gyr through F1042M. The black curves are the same photometric detection limits shown in Fig. 5. The horizontal lines represent the apparent brightnesses of brown dwarfs with masses 40 (*solid lines*), 30 (*long-dashed lines*), 20 (*long-dash–short-dashed lines*), 10 (*short-dashed lines*), and 5 M_J (*dotted line*) and with distances 1 (*red lines*) and 5 pc (*blue lines*). The F1042M magnitudes of the brown dwarfs were determined using the predicted J magnitudes from the models of Burrows et al. (1997) and an assumed constant value of $m_{1042} - J = 1$ for all brown dwarfs within the considered ranges of mass and age. See text for details and caveats.

magnitudes of brown dwarfs with masses 5–40 M_J (1 $M_J \approx 0.001\ M_\odot$) at distances of 1 pc (*red lines*) and 5 pc (*blue lines*). Note that 21 of our 23 targets lie at distances $\lesssim 5$ pc. For a target of given brightness, our F1042M images would reveal all brown dwarfs represented by the horizontal line segments located above and to the right of the appropriate photometric detection limit. For example, we can approximate our sensitivity to any brown dwarf companions of Gl 559A (α Centauri A; $m_{1042} = 0.01$, $d = 1.3$ pc) by inspecting the red (1 pc) lines above and to the right of the black curve labeled "mag ~ 0.2" in Figure 5. In this case, 40 M_J brown dwarfs aged 0.5, 1.0, and 5.0 Gyr would have been detected at separations beyond approximately $1\rlap{.}''75$, $2\rlap{.}''5$, and $5''$, respectively. For Gl 551 (Proxima Centauri; $m_{1042} = 6.00$, $d = 1.3$ pc), a 5 M_J brown dwarf companion (or gaseous giant planet) aged 0.5 Gyr would have been detected as close as $\sim 2''$ (2.6 AU) from the star. Figure 12 indicates that our search is not sensitive to 1 Gyr–old brown dwarfs with masses $\lesssim 5\ M_J$ at any distance. Likewise, Figure 13 indicates an insensitivity to 5 Gyr–old brown dwarfs with masses $\lesssim 10\ M_J$ at any distance.

Because the atmospheric models of Burrows et al. (1997) do not accurately reproduce the optical spectrum of Gl 229B (A. Burrows 1999, private communication), our assumption of constant proportionality between the F1042M and J-band fluxes for brown dwarfs of the ages and masses under consideration (and Figures 11–13, which are based upon that assumption) must be treated with caution. Fortunately, the disagreement between obser-
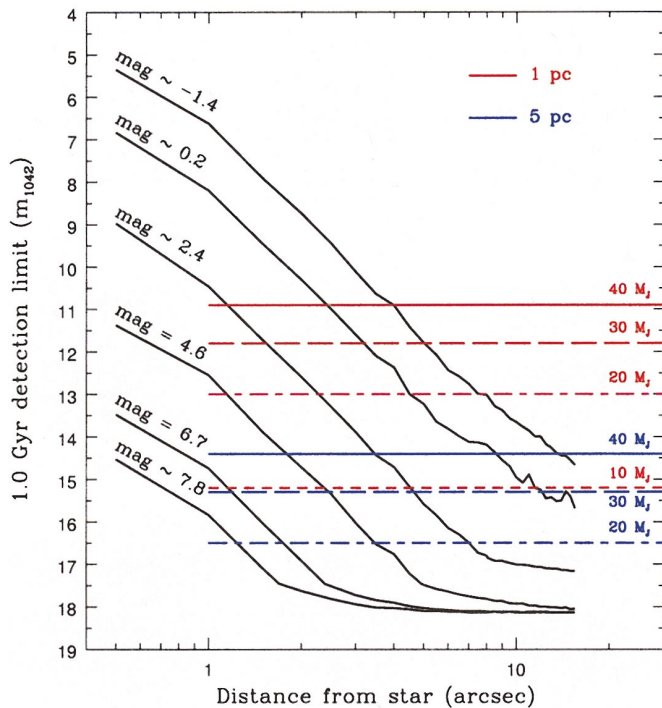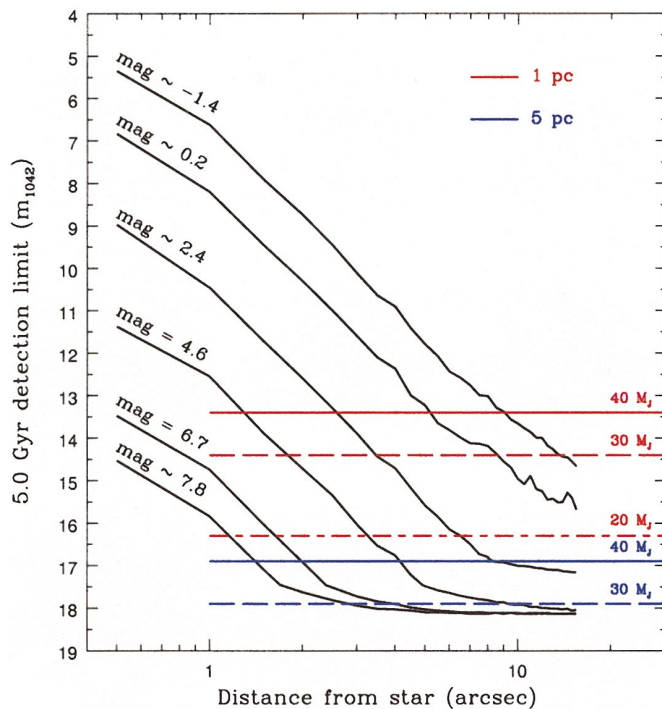
Fig. 12.—Theoretical limits of sensitivity to brown dwarfs aged 1.0 Gyr through F1042M. All curves are as described in the legend to Fig. 11. At 1 Gyr, our search is no longer sensitive to 5 M_J brown dwarfs.

vation and theory tends to increase shortward of 0.9 μm (Schultz et al. 1998a; Golimowski et al. 1998), so our estimated sensitivities at 1 μm, though crude, should not be grossly inaccurate.

Fig. 13.—Theoretical limits of sensitivity to brown dwarfs aged 5.0 Gyr through F1042M. All curves are as described in the legend to Fig. 11. At 5 Gyr, our search is no longer sensitive to 10 M_J brown dwarfs.

4.2. Implications of Null Result

The promotion by *Hipparcos* (ESA 1997) of Gl 887 to the 10th nearest star system and the demotions of Gl 845 and Gl 71 to the 18th and 19th nearest systems, respectively, undermined our attempt to search for FCs to the 17 nearest systems. (The subsequent failure of our observations of Gl 845 did not further affect this strategy.) Because our final list of target stars is neither large nor volume limited nor uniformly imaged, assessing the significance of our null result in a formal statistical sense is impracticable. Moreover, the ages of our target stars are not well constrained, so a rigorous comparison of our null result with the number of brown dwarfs expected from evolutionary models and some companion mass function is precluded. These limitations, however, do not prevent a few qualitative comments regarding the lack of new detections.

Our search revealed no stellar companions with spectral types later than M6 V around 17 of the 19 nearest star systems. Ten of these systems (Gl 15AB, Gl 65AB, Gl 406, Gl 411, Gl 447, Gl 699, Gl 725AB, Gl 729, Gl 866ABC, and Gl 905), all of which comprise early- to mid-M dwarfs, were imaged previously to limits at or below the end of the main sequence for separations of ~1–10 AU (Henry & McCarthy 1990) and ~100–1000 AU (Simons et al. 1996). Based on an average distance to these ten systems of 2.95 pc, our search covered separations of ~1–50 AU from these stars to depths beyond the end of the main sequence. Thus, except for separations of ~50–100 AU, these ten stars have been searched for VLM companions from 1 AU to the limits of gravitationally bound orbits with no result. The apparent lack of companions with spectral types later than M6 V supports the evidence that M dwarfs favor binary systems of nearly equal masses (Reid & Gizis 1997a).

The absence of any substellar companions to our target stars suggests that any or all of the following situations exist in the immediate solar neighborhood: (1) the formation of star–brown dwarf multiples is greatly suppressed by some physical mechanism; (2) brown dwarfs cool much more rapidly than predicted by current evolutionary models; and (3) the ages of the systems studied by us exceed 5 Gyr, at which time even the most massive brown dwarfs would have faded below the sensitivity limits of our search. The first two options have been discussed by Simons et al. (1996). The third option is not likely for our entire sample, as both space motion and chromospheric activity indicate youth relative to the Sun for some targets (Leggett 1992; Henry et al. 1996; Delfosse et al. 1998). Oppenheimer (1999) has noted that the tendency toward equal-mass binaries near the end of the main sequence may apply to brown dwarfs as well, and that the apparent paucity of substellar companions may simply be an artifact of the currently small number of known isolated brown dwarfs. If so, then the first unambiguous discovery of a brown dwarf—a companion to the M1 V star Gl 229 (Nakajima et al. 1995)—may have been an extraordinary fluke.

5. SUMMARY AND CONCLUSIONS

We have completed a direct-imaging search for faint companions (FCs) to 23 stars within 13 pc of the Sun using the *HST* Planetary Camera. Images obtained through the F1042M (1 μm) and F814W (*I*-band) filters provided sensitivity to FCs at separations of 0″.5–17″ (~1–60 AU, for an average distance of 3.7 pc) to an ultimate 10 σ detection

limit of $m_{1042} \approx 18$. As the end of the main sequence occurs at $M_{1042} \approx 12$, this detection limit makes our search for FCs to nearby stars the most sensitive yet published. Despite this great sensitivity, no previously undetected FCs were found.

We present the first direct image of the triple system GJ 1245ABC in which all three components are well resolved. Multiband photometry of GJ 1245C suggests for that object a spectral type later than M7. The measured positions of GJ 1245AC are discordant with those expected from published photocentric-orbit elements. However, our positions do agree with those measured interferometrically with *HST*'s FGS, from which the latest and most precise values of the masses have been derived. The observed positions of four other multiple systems (Gl 65AB, Gl 244AB, Gl 280AB, and Gl 866ABC) also differ from those expected from published orbital elements. The discrepancies noted for Gl 280AB are sufficient to resolve the long-standing inconsistency between Procyon's observed luminosity and that derived from the theoretical MLR.

Our images of the astrometric binary Gl 105A do not reveal the presence of a fourth component, as has been proposed to reconcile the differences between the observed location of the M7 V companion Gl 105C and the predicted separations of the perturbing body from two independent astrometric studies. A photometric and astrometric analysis of Gl 105C itself will be presented in a forthcoming paper.

Our survey would have detected all stellar companions within $17''$ of our target stars except for any lowest mass companions lying within $0.''5–1''$ of the brightest ($V < 1.5$) targets. The absence of companions with spectral types later than M6 around 17 of the nearest 19 systems (the other two systems were not included in the survey) supports recent evidence that M dwarfs favor binary systems of nearly equal masses.

Applying recent models of brown dwarf spectra and evolution, we find that our search was sensitive to young (0.5 Gyr), low-mass (less than 10 M_J) brown dwarf companions to the fainter targets within 5 pc. A brown dwarf with mass 40 M_J and age 5 Gyr would have been detected at separations greater than $5''$ from Gl 559A (α Centauri A). Our search was not sensitive to 1 Gyr–old brown dwarfs with masses $\lesssim 5\ M_J$, nor was it sensitive to 5 Gyr–old brown dwarfs with masses $\lesssim 10\ M_J$.

The absence of any substellar companions to our target stars suggests any or all of the following: (1) the formation of brown dwarfs as companions to stars is somehow inhibited; (2) brown dwarfs cool more rapidly than expected; and (3) the targets of our search are much older than 5 Gyr, so any substellar companions would have faded below our detection limit. Although the ages of our target stars are not well constrained, there exists evidence that some are young relative to the Sun. Option 3 is therefore unlikely.

REFERENCES

Baggett, S. 1995, in Space Telescope Analysis News: WFPC2, No. 3, ed. D. Golombek (Baltimore: STScI)
Benedict, G. F., et al. 1999, AJ, 118, 1086
Benest, D., & Duvent, J. L. 1995, A&A, 299, 621
Bond, H. E., Gilliland, R. L., Schaefer, K. G., & Girard, T. M. 1999, in ASP Conf. Ser. 169, 11th European Workshop on White Dwarfs, ed. J.-E. Solheim & E. G. Meištas (San Francisco: ASP), 297
Burrows, A., Hubbard, W. B., Saumon, D., & Lunine, J. I. 1993, ApJ, 406, 158
Burrows, A., et al. 1997, ApJ, 491, 856
Burrows, C. J., et al. 1995, *Hubble Space Telescope*: Wide Field Planetary Camera 2 Instrument Handbook (version 3.0; Baltimore: STScI)
Campbell, B., Walker, G. A. H., & Yang, S. 1988, ApJ, 331, 902
Delfosse, X., Forveille, T., Beuzit, J.-L., Udry, S., Mayor, M., & Perrier, C. 1999, A&A, 344, 897
Delfosse, X., Forveille, T., Perrier, C., & Mayor, M. 1998, A&A, 331, 581
ESA. 1997, The *Hipparcos* and Tycho Catalogues (ESA SP-1200) (Noordwijk: ESA)
Gatewood, G. 1996, BAAS, 28, 885
Gatewood, G. D. 1995, Ap&SS, 223, 91
Geyer, D. W., Harrington, R. S., & Worley, C. E. 1988, AJ, 95, 1841
Gliese, W., & Jahreiss, H. 1991, Preliminary Version of the Third Catalogue of Nearby Stars (NSSDC/ADC Cat. 5070A) (Greenbelt, MD: GSFC) (CNS3)
Golimowski, D. A., Burrows, C. J., Kulkarni, S. R., Oppenheimer, B. R., & Brukardt, R. A. 1998, AJ, 115, 2579
Golimowski, D. A., Fastie, W. G., Schroeder, D. J., & Uomoto, A. 1995a, ApJ, 452, L125
Golimowski, D. A., Nakajima, T., Kulkarni, S. R., & Oppenheimer, B. R. 1995b, ApJ, 444, L101
Golimowski, D. A., & Schroeder, D. J. 1998, AJ, 116, 440
Harrington, R. S. 1990, AJ, 100, 559
Hawley, S. L., Gizis, J. E., & Reid, I. N. 1996, AJ, 112, 2799
———. 1997, AJ, 113, 1458
Heintz, W. D., & Cantor, B. A. 1994, PASP, 106, 363
Henry, T. J., Franz, O. G., Wasserman, L. H., Benedict, G. F., Shelus, P. J., Ianna, P. A., Kirkpatrick, J. D., & McCarthy, D. W. 1999, ApJ, 512, 864

Henry, T. J., Kirkpatrick, J. D., & Simons, D. A. 1994, AJ, 108, 1437
Henry, T. J., & McCarthy, D. W. 1990, ApJ, 350, 334
Henry, T. J., Soderblom, D. R., Donahue, R. A., & Baliunas, S. L. 1996, AJ, 111, 439
Holtzman, J. A., Burrows, C. J., Casertano, S., Hester, J. J., Trauger, J. T., Watson, A. M., & Worthey, G. 1995a, PASP, 107, 1065
Holtzman, J. A., et al. 1995b, PASP, 107, 156
Ianna, P. A. 1992, in ASP Conf. Ser. 32, Complementary Approaches to Double and Multiple Star Research, ed. H. A. McAlister & W. I. Hartkopf (IAU Coll. 135) (San Francisco: ASP), 323
Irwin, A. W., Fletcher, J. M., Yang, S. L. S., Walker, G. A. H., & Goodenough, C. 1992, PASP, 104, 489
Jameson, R. F., Sherrington, M. R., & Giles, A. B. 1983, MNRAS, 205, 39P
Krist, J. E. 1995, in Calibrating *Hubble Space Telescope*: Post Servicing Mission, ed. A. Koratkar & C. Leitherer (Baltimore: STScI), 311
———. 2000, WFPC2 Instrum. Sci. Rep., in preparation
Krist, J. E., Golimowski, D. A., Schroeder, D. J., & Henry, T. J. 1998, PASP, 110, 1046
Krist, J., & Hook, R. 1997, The Tiny Tim User's Guide (version 4.4; Baltimore: STScI)
Leggett, S. K. 1992, ApJS, 82, 351
Leggett, S. K., Allard, F., & Hauschildt, P. H. 1998, ApJ, 509, 836
Leinert, C., Haas, M., Allard, F., Wehrse, R., McCarthy, D. W., Jahreiss, H., & Perrier, C. 1990, A&A, 236, 399
Leinert, C., Henry, T., Glindemann, A., & McCarthy, D. W. 1997, A&A, 325, 159
Lippincott, S. L. 1983, PASP, 95, 775
Lowrance, P. J., et al. 1999, ApJ, 512, L69
Matthews, K., Nakajima, T., Kulkarni, S. R., & Oppenheimer, B. R. 1996, AJ, 112, 1678
McCarthy, D. W., Henry, T. J., Fleming, T. A., Saffer, R. A., & Liebert, J. 1988, ApJ, 333, 943
Nakajima, T., Durrance, S. T., Golimowski, D. A., & Kulkarni, S. R. 1994, ApJ, 428, 797
Nakajima, T., Oppenheimer, B. R., Kulkarni, S. R., Golimowski, D. A., Matthews, K., & Durrance, S. T. 1995, Nature, 378, 463
Nelson, A. F., & Angel, J. R. P. 1998, ApJ, 500, 940
Oppenheimer, B. R. 1999, Ph.D. thesis, Caltech

Probst, R. G., & O'Connell, R. W. 1982, ApJ, 252, L69
Reid, I. N., & Gizis, J. E. 1997a, AJ, 113, 2246
———. 1997b, AJ, 114, 1992
Rudy, R. J., Rossano, G. S., & Puetter, R. C. 1996, ApJ, 458, L41
Schroeder, D. J., & Golimowski, D. A. 1996, PASP, 108, 510 (Paper I)
Schultz, A. B., et al. 1998a, ApJ, 492, L181
———. 1998b, AJ, 115, 345
Simons, D. A., Henry, T. J., & Kirkpatrick, J. D. 1996, AJ, 112, 2238
Skrutskie, M. F., Forrest, W. J., & Shure, M. 1989, AJ, 98, 1409
Tsuji, T., Ohnaka, K., & Aoki, W. 1999, ApJ, 520, L119

van Altena, W. F., Lee, J. T., & Hoffleit, E. D. 1995, The General Catalogue of Trigonometric Stellar Parallaxes, Vols. 1 and 2 (4th ed.; New Haven: Yale Univ. Obs.)
van Buren, D., Brundage, M., Ressler, M., & Terebey, S. 1998, AJ, 116, 1992
van de Kamp, P. 1986, Space Sci. Rev., 43, 211
Walker, G. A. H., Walker, A. R., Irwin, A. W., Larson, A. M., Yang, S. L. S., & Richardson, D. C. 1995, Icarus, 116, 359
Weis, E. W. 1996, AJ, 112, 2300
Zuckerman, B., & Becklin, E. E. 1992, ApJ, 386, 260